ARTICLE **Open Access**

Chemically and electronically active metal ions on InAs quantum dots for infrared detectors

Seongchan Kim[1], Sooyeon Yeon[1], Minwoo Lee[1], Junyoung Jin[2], Seungki Shin[1], Namyoung Gwak[1], Inyoung Jeong[1], Hyunwoo Jang[1], Gyu Weon Hwang [2] and Nuri Oh [1]

Abstract

Colloidal InAs quantum dots (QDs) are emerging candidates for NIR-SWIR optoelectronic applications because of their excellent electrical and optical properties. However, the syntheses of InAs QDs, which demand strongly reducing atmospheres or highly reactive precursors, are difficult because of their highly covalent bonding and lack of Group 15 precursors. While the coreduction method with commercially available arsenic precursors enables facile syntheses of InAs QDs, it results in broad size distributions requiring subsequent size-selection processes. In this study, we introduced zinc ions in the form of coordination complexes during coreduction of the indium and arsenic precursors. The Zn ions chemically passivated the surfaces of the InAs QDs, narrowed the size distribution and removed surface defects. When the InAs QDs were integrated into infrared photodiodes as IR absorbers, the surface-attached Zn ions electrically modulated the energy level and carrier concentration. Infrared photodiodes with the InAs:Zn QD layers exhibited dark currents and photoresponses that were two orders of magnitude lower and approximately twice as fast, respectively, as those seen for bare InAs QDs.

Introduction

Indium arsenide (InAs) is a III–V compound semiconductor with a small effective carrier mass, direct bandgap, and small exciton binding energy, which are attractive properties for state-of-the-art electronic and optoelectronic applications[1,2]. Owing to the quantum confinement effect, nanosized crystals of InAs have additional benefits, including tunable optical bandgaps ranging from the near-infrared (NIR) to the short wavelength infrared (SWIR) and versatile solution processability[3–5]. Given these advantages, InAs quantum dots (QDs) can be formed into thin solid forms and integrated into various IR photosensors used for machine vision, imaging sensors, and telecommunications[6–8]. To achieve high-performance QD-based NIR

or SWIR photodetectors, it is important to obtain highly monodisperse InAs QDs and limit surface defects, which enhances the charge transport properties of the QD film[9].

However, the syntheses of InAs QDs are not as simple as those of ionic compound semiconductor nanocrystals because of the highly covalent bonding between indium and arsenic and the lack of accessible arsenic precursors[10,11]. Previous studies using continuous injection and seeded growth methods have been focused on controlling the reactivities of highly reactive silylated or germylated arsenic precursors, such as tris-trimethylsilylarsine and tris-trimethylgermyl arsine, which are difficult to handle owing to their toxicities and pyrophoricities[12,13]. Additionally, the coreduction method with commercially available arsenic precursors, such as arsenic chloride and tris-dimethylaminoarsine, could be another facile approach for InAs QD syntheses[14,15]. A simple heating process, along with simultaneous reduction of the indium and arsenic precursors, may be suitable for large-scale production; however, it generally requires a subsequent

Correspondence: Nuri Oh (irunho@hanyang.ac.kr)
[1]Division of Materials Science and Engineering, Hanyang University, 222, Wangsimni-ro, Seongdong-gu, Seoul 04763, Republic of Korea
[2]Center for Neuromorphic Engineering, Korea Institute of Science and Technology, 5 Hwarang-ro 14-gil, Seongbuk-gu, Seoul 02792, Republic of Korea
These authors contributed equally: Seongchan Kim, Sooyeon Yeon

size-selection process because it produces a broad size distribution in the resultant QDs. In addition, as with other nanoscale III–V semiconductors, the surfaces of InAs QDs are prone to oxidation[11,16]. During the synthetic procedure, oxidative defects must be avoided so the QDs have homogeneous optoelectronic properties.

Recent studies have revealed that additional ions, including those of metals, chalcogens, and halogens, play critical roles in controlling the structural and optical properties of III–V QDs[16,17]. These ions can be introduced into the QD solution during either the synthetic or postsynthetic process. In particular, the effects of Zn addition during the synthesis of indium phosphide (InP) QDs, which presumably possess surface characteristics similar to those of InAs, have been widely studied. The addition of Zn precursors to the InP QDs improved the size uniformity and consequently reduced the bandwidths of the absorption and emission spectra of the InP QDs[18]. The Zn ions incorporated into the InP lattice and on the InP surface improved the photoluminescence properties by reducing the number of surface defect states[19,20] or alleviating lattice mismatches between the core and shell[21,22]. These results indicate that transition metal ions could be employed as reaction additives during the QD synthesis, resulting in efficient surface passivation, enhanced optical properties, and improved size uniformity of the III–V QDs[23].

In the case of InAs QDs, the incorporation of additional ions has been conducted mainly through postsynthetic treatments. Posttreatment with cadmium oleate changed the electrical properties of InAs QD films and protected the surfaces of InAs QDs from oxidation[24]. Hydrogen sulfide vapor treatment of InAs QD films also tuned the electrical properties and improved their stability in air[25]. These additional ions were chemically adsorbed on the surface of the QDs and acted as electrical dopants. However, there have been insufficient methodological studies to improve the properties of InAs QDs during the synthetic process. The addition of Zn precursors during seeded growth of the InAs/ZnSe core/shell QDs improved the emission properties; however, the mechanism for the reaction between Zn and the InAs core has not been elucidated[26,27].

In this work, we describe a synthetic strategy using zinc chloride-based reaction additives for the syntheses of InAs QDs, which improved the monodispersity of the InAs QDs and simultaneously enhanced their optoelectronic properties by removing surface oxidized species. We introduced Zn coordination complexes into the indium and arsenic reaction mixture, and those appeared to be indirectly involved in the reaction between the In and As precursors. The Zn ions eventually passivated the surfaces of the resultant InAs QDs, improved the colloidal stability and facilitated the fabrication processes for follow-up

devices. As the surface Zn ions also affected the electrical properties and energy levels of InAs QD films, IR photodiodes incorporating the InAs with Zn QD assembly showed a dark current that was two orders of magnitude lower than that of bare InAs QDs and efficiently detected NIR/SWIR light at 1050 nm.
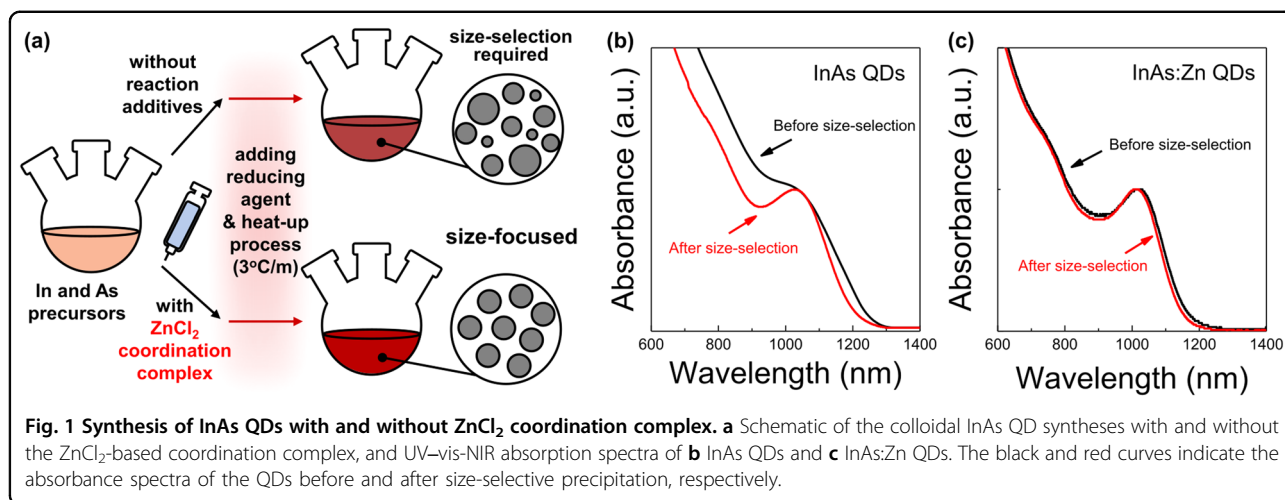
Materials and methods
Materials
Indium (III) chloride (anhydrous, 99.999%) was purchased from Strem Chemicals. Arsenic(III) chloride (99.99%, trace metals basis), oleylamine (OLAM, 70%, technical grade), lithium triethylborohydride (LiEt$_3$BH, superhydride, 1.0 M solution in THF), dioctyl ether (DOE, 99%), trioctylphosphine (TOP, 97%), zinc chloride (99.999%, trace metals basis), zinc bromide (99.999%, trace metals basis), zinc iodide (anhydrous, power, 99.999% trace metals basis), molybdenum(VI) oxide (MoO$_3$, ACS reagent, ≥99.5%), tetrachloroethylene (TCE, anhydrous, ≥99%), acetonitrile (anhydrous, 99.8%), toluene (anhydrous, 99.8%), and octane (anhydrous, ≥99%) were purchased from Sigma–Aldrich.

Synthesis of InAs QDs
The InAs QDs were synthesized via a modified coreduction method using an As precursor with oleylamine. InCl$_3$ (1 mmol) and AsCl$_3$ (5 mmol) were dissolved in 20 ml of predegassed OLAM and stirred overnight at ~60 °C in a glovebox. ZnCl$_2$ (10 mmol) was dissolved in TOP (10 ml) and stirred for two days at 80 °C in a glovebox. For the reducing agents, the preparation processes were the same as in the previous method. A 2 M solution of superhydride (LiEt$_3$BH in THF) in predegraded dioctyl ether was prepared. Before the synthesis, 10 ml of a 0.05 M indium precursor solution, 1 ml of 0.25 M As precursor solution, and a certain ratio of the zinc chloride complex precursor were mixed in a three-necked flask under an inert atmosphere. After 1.25 ml of 2 M superhydride was injected into the reaction flask, the mixture turned dark, and bubbles were generated. The reaction flask was then heated to the reaction temperature at 3 °C/min and maintained at that temperature for 15 min. After growth, the reaction was quenched quickly, and the product was transferred to a glovebox without air exposure for purification. For purification, 30 ml of toluene was added to the reaction mixture, which was then transferred into two centrifuge tubes. The dispersion was then centrifuged at 5000 rpm for 5 min. Acetonitrile (12 ml) was then added to each supernatant with subsequent centrifugation. The aggregates were then dissolved in 5 ml of toluene and centrifuged at 5000 rpm for 5 min after adding ethanol to the solution until it turned turbid. Finally, the aggregates were redispersed in octane after centrifugation.

Fig. 1 Synthesis of InAs QDs with and without ZnCl₂ coordination complex. a Schematic of the colloidal InAs QD syntheses with and without the ZnCl₂-based coordination complex, and UV–vis-NIR absorption spectra of **b** InAs QDs and **c** InAs:Zn QDs. The black and red curves indicate the absorbance spectra of the QDs before and after size-selective precipitation, respectively.

Photodiode device fabrication

An ITO glass substrate was cleaned in an ultrasonic bath for 30 min, first with acetone and then with isopropyl alcohol. The substrate was then treated with an ultraviolet (UV) ozone cleaner for 15 min. After cleaning, ZnO nanoparticles, which were synthesized by a sol-gel process using zinc acetate dihydrate and methyl alcohol, were spin-coated onto the ITO substrate at 2000 rpm for 30 s and annealed in air at 300 °C for 40 min. InAs QDs redispersed in octane (100 mg/ml) were spin-coated onto the substrate and annealed at 200 °C for 30 min in a glovebox. MoO_3 and Au layers were deposited at thicknesses of 10 and 120 nm, respectively, using a thermal evaporator. All devices were encapsulated with cover glasses and UV-cured epoxy.

Characterizations

For ultraviolet–visible NIR (UV–vis-NIR) absorption measurements, the synthesized InAs QDs were dispersed in TCE. Absorption spectra were obtained with a SHIMADZU UV-2600 UV–vis-NIR spectrometer (200–1400 nm). XRD measurements were performed with a miniFlex 600 diffractometer (RIGAKU) with a Cu Kα source operated at 40 kV and 15 mA in scanning mode. InAs QDs dispersed in hexane were drop-cast on an XRD glass holder (RIGAKU). The sample for TEM imaging was dissolved in hexane and drop-cast onto a carbon-coated 300 mesh copper TEM grid. TEM images were captured with a JEOL JEM-2010 system operating at 200 kV. ICP–OES measurements were performed with an ICAP 7000 SERIES instrument (Thermo Fisher Scientific). UPS measurements were performed with an XPS-Theta Probe (Thermo Fisher Scientific). InAs QDs dispersed in octane were drop-cast on 1.0 cm × 1.0 cm silicon substrates and baked at 200 °C for 30 min in a glove box. During the UPS measurements, a helium discharge source (He 1α = 21.22 eV) was used, and the samples were kept at high pressure. The work function was calculated

with the equation:

$$W_F = 21.22 - E_{\text{cut off}}(\text{eV})$$

For the bandwidth measurements, a frequency modulated 808 nm laser diode with a function generator (HP 33120A) and a lock-in amplifier (SR830) were used. The noise spectral density was measured with an SR570 low-noise preamplifier and Advantest R9221B. The dark current and responsivity of the photodiode devices were characterized with a source-meter (Keithley 2602) and function generator (Agilent 33220A) during illumination with a 1050 nm laser diode.

Results and discussion

In the synthesis of the InAs QDs (Fig. 1a), we employed a modified coreduction method that included commercial indium and arsenic chloride precursors dissolved in oleylamine[28]. The coreduction method has the advantages of simplicity and facile scalability for the production of QDs[29]. However, the resultant QDs showed a wide size distribution, and thus, a size-selective precipitation process was required to select the appropriately sized QDs[2,14,28]. Figure 1b shows absorption spectra of the conventional InAs QDs synthesized at 300 °C using the standard coreduction method, and these were obtained before and after the size selection process. Before size selection (black line), the absorption spectrum had a featureless broad peak with a tail, indicating the heterodispersity of the InAs QDs. After removing the relatively small and large InAs particles, the absorbance ratio between the excitonic peak and the valley (peak-valley ratio), a parameter used to confirm the uniformities of the QD sizes and shapes, was 0.87, indicating a narrower size distribution for the InAs QDs[30]. In this regard, the InAs nucleation process did not seem to be completely

suppressed but continued to occur even during the growth periods.

To address this problem in the coreduction method, we employed reaction additives to modify the nucleation and growth processes, which improved the dispersity and uniformity without a follow-up size-selection process. The broad size distribution was attributed to surface-reaction-controlled growth due to the strong covalent bonding between the In and As ions, which impeded surface reactions on the InAs nuclei[31]. In our synthetic method, the In and As precursors were chemically reduced immediately after injection of the reducing agent and diffused to the surfaces of the InAs nuclei as the reaction temperature increased. The slow surface reaction of the In and As precursors determined the growth rate of InAs QDs; therefore, we considered reaction additives to alter the reaction path and improve the surface reaction rate.
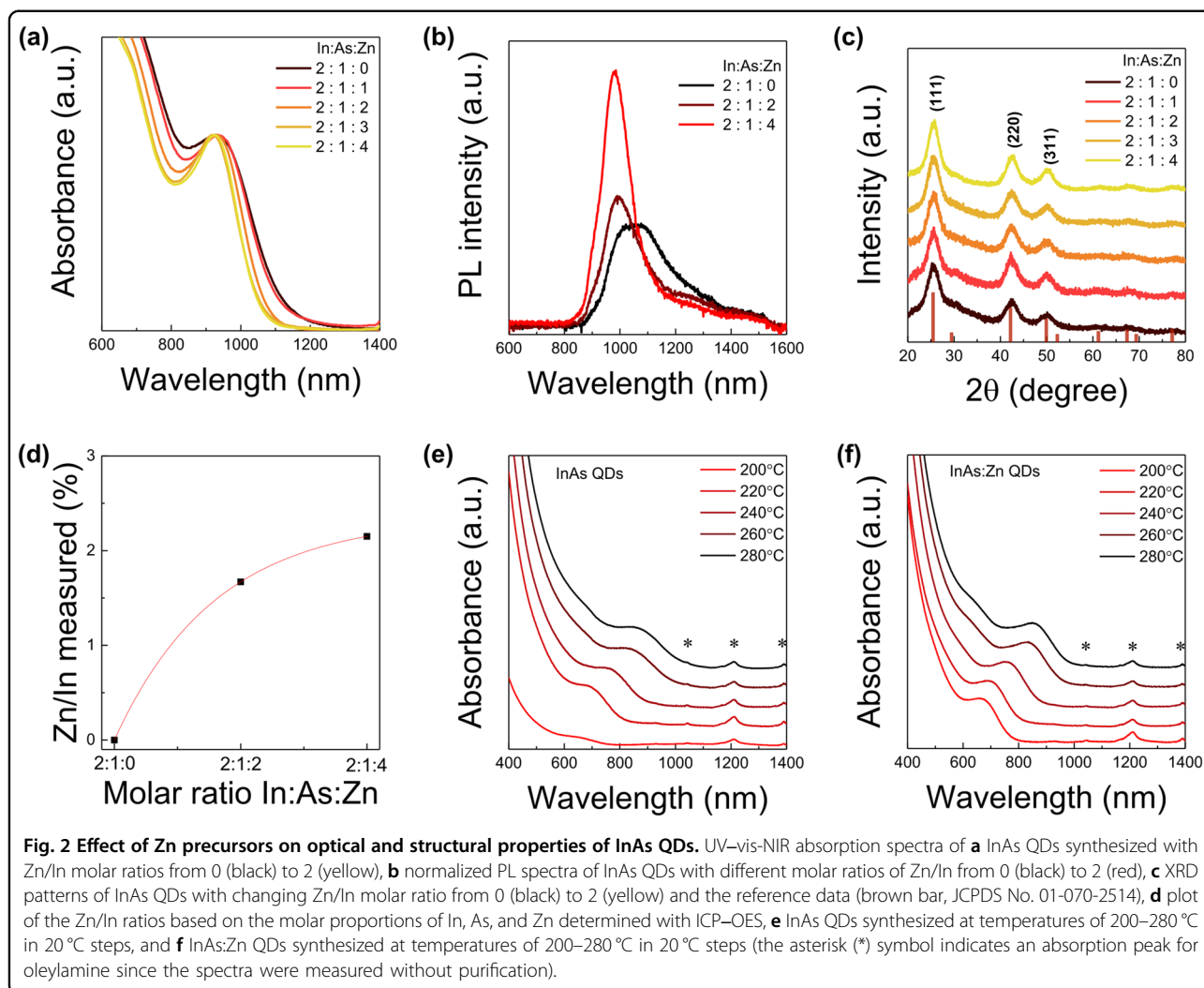
Based on previous studies of the syntheses of InP QDs that incorporated Zn, zinc chloride could be an effective additive in changing the precursor reactivities and passivating the surfaces of III-V QDs[22,30,32]. Because Zn and Cl ions are reactive, they aggressively replace the native surface ligands of the InAs nucleates. Instead, we used a zinc chloride-based coordination complex prepared by mixing a 1:2 molar ratio of zinc chloride and tri-n-octylphosphine ($ZnCl_2$-TOP)[33]. We synthesized InAs along with the $ZnCl_2$-TOP precursor before injecting the reducing agent, but kept the other reaction conditions unchanged (Fig. 1a). As shown in Fig. 1c, regardless of the follow-up process, the absorption spectra of the InAs QDs synthesized with the $ZnCl_2$-TOP precursor (referred to as InAs:Zn QDs) showed distinct excitonic peaks and similar peak-to-valley ratios of 0.78. Addition of the $ZnCl_2$-TOP precursor improved the size uniformity of the InAs QDs without altering their optical properties. A recent study reported the effects of $ZnCl_2$ on the syntheses of InAs QDs. However, the Zn precursor complex that we used was more stable than $ZnCl_2$, even at temperatures above 200 °C at which the InAs nuclei were formed. In addition, the direct use of $ZnCl_2$ may induce the formation of Zn ions and yield ZnAs or Zn_3As_2 particles. We believe that the $ZnCl_2$-TOP complex effectively facilitated the nucleation and growth processes of InAs, even at high temperatures.

We theorize an indirect role for the $ZnCl_2$-TOP precursors in the formation of InAs. Pnictogen elements such as P, As, and Sb are known to form Zintl phases, which are polyanionic clusters[34,35]. Homoatomic units, such as $[As_7]^{3-}$, often form coordination compounds with transition metals, such as Zn, Cd, and Cs. For example, Zn ions were seen to bridge two $[As_7]^{3-}$ units to yield isolated $[Zn(As_7)_2]^{4-}$ anions, which were subsequently stabilized and generally solvated by Group I metal ions, such

as Li^+ and Na^+ cations. These zinc-coordinated Zintl anions could be the intermediate states of the As precursors leading to InAs formation, especially in the strong reducing atmosphere formed by $Li(C_2H_5)_3BH$. We believe that the intermediate phases induced by the $ZnCl_2$-TOP precursor likely retarded the formation of pure arsenic precipitates and increased the reaction rate of As with In ions. The reaction between the Zn and As precursors was confirmed by the formation of zinc-arsenic particles. During a similar coreduction reaction with only Zn and As precursors in the presence of a reducing agent, Zn-As particles were formed at elevated temperatures (Fig. S1a). The indirect band gap of the zinc arsenide particles generated a broad absorption peak in the 700−800 nm range (Fig. S1b), and the XRD pattern of the particles indicated low crystallinity, presumably due to the mixed growth of Zn_3As_2 and $ZnAs_2$ (Fig. S1c).

To elucidate the effect of the $ZnCl_2$-TOP precursor on the resultant InAs structure, we synthesized InAs QDs with different molar ratios of Zn and In/As precursors at a reaction temperature of 300 °C. Figure 2 shows the UV−vis-NIR absorption spectra, photoluminescence (PL) spectra, and XRD patterns of the InAs QDs made with various concentrations of the $ZnCl_2$-TOP precursor. As the Zn/In molar ratio was increased from 0 to 2, the absorption spectra showed a deep valley with a sharp excitonic peak, which corresponded to a change in the peak-to-valley ratio from 0.93 to 0.74 without the size-selection process (Fig. 2a). With increasing amounts of the Zn precursor, a slight blueshift in the absorption peak from 936 to 926 nm was observed. However, the small shift did not indicate a significant size change but rather indicated the disappearance of relatively large QDs. The deep valley in the absorption curve also revealed that the fraction of relatively small InAs QDs had diminished. Size focusing was observed when the reaction temperature was increased to 330 °C to obtain large InAs QDs (Fig. S2).
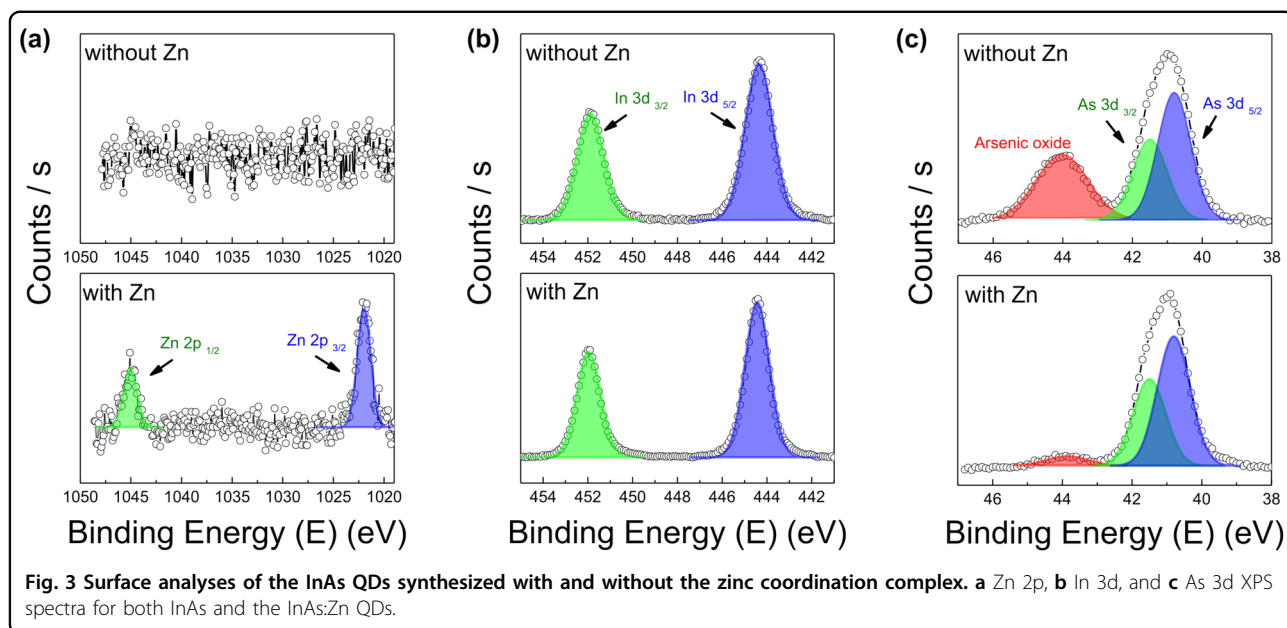
In addition to the size focusing effect, the $ZnCl_2$-TOP precursor also influenced the luminescence properties of the InAs QDs, as shown in the PL spectra (Fig. 2b). While distinct infrared light emission was observed from both InAs and InAs:Zn QDs, the InAs:Zn QDs exhibited a higher peak intensity and narrower emission bandwidth than the bare InAs QDs. The PLQY of the InAs:Zn QDs was 1.26 ± 0.4%, and this was higher than the PLQY of the bare InAs QDs, which is generally less than a few percent and was often reported as less than 1% (or not observed at all) in previous studies[27,28]. Additionally, the InAs:Zn QDs had a narrower full width at half-maximum (FWHM) of approximately 120 nm compared to the InAs QDs with a FWHM greater than 280 nm, as shown in Fig. S2. The narrow emission spectra and high PLQY of the InAs:Zn QDs are attributed to their uniform sizes and are affected by the reduced trap states. The trap emission ranging

Fig. 2 Effect of Zn precursors on optical and structural properties of InAs QDs. UV–vis-NIR absorption spectra of **a** InAs QDs synthesized with Zn/In molar ratios from 0 (black) to 2 (yellow), **b** normalized PL spectra of InAs QDs with different molar ratios of Zn/In from 0 (black) to 2 (red), **c** XRD patterns of InAs QDs with changing Zn/In molar ratio from 0 (black) to 2 (yellow) and the reference data (brown bar, JCPDS No. 01-070-2514), **d** plot of the Zn/In ratios based on the molar proportions of In, As, and Zn determined with ICP–OES, **e** InAs QDs synthesized at temperatures of 200–280 °C in 20 °C steps, and **f** InAs:Zn QDs synthesized at temperatures of 200–280 °C in 20 °C steps (the asterisk (*) symbol indicates an absorption peak for oleylamine since the spectra were measured without purification).

from 1100 to 1400 nm decreased as the amount of $ZnCl_2$-TOP precursor was increased. There are two possible causes for this phenomenon: surface trap states, such as In and As dangling bonds, were passivated, and/or the unavoidable oxidative species formed on the surface were removed by the precursors. These changes in the surface states as well as the chemical analyses will be discussed in a later section.

Crystal structure analyses can reveal whether the InAs QDs synthesized with the $ZnCl_2$-TOP precursors were alloyed. In the X-ray diffraction (XRD) measurements, all of the InAs QDs synthesized at 300 and 330 °C with various molar ratios of the added Zn precursor had zinc-blende crystal structures with peaks at 25.54°, 42.33°, and 50.1° corresponding to the (111), (220), and (311) planes, respectively (Figs. 2c and S4). If an InZnAs alloy had formed, the XRD patterns would have broad shapes or shifts to higher angles. However, the lattice parameters and crystal structures did not change, even when the

molar amount of the added Zn precursor was twice as high as that of In. To confirm the elemental composition, inductively coupled plasma–optical emission spectrometry (ICP–OES) was applied to the purified InAs and InAs:Zn QDs. As the amount of the $ZnCl_2$-TOP precursor was increased, the detected Zn:In ratio increased (Fig. 2d). However, the molar amount of Zn detected for the InAs:Zn QDs was much less than that in the $ZnCl_2$-TOP precursor used for the synthesis, in contrast to a previous study on InP QD synthesis from a Zn precursor (Table S1). We believe that the Zn ions were located on the surfaces of the InAs QDs, or if not, they diffused out to the surface via a self-purification process[36]. An estimate based on the amount of Zn detected showed that approximately 8–10 Zn atoms were adsorbed on a single InAs QD. The Zn ions possibly passivated the As dangling bonds to improve the chemical and colloidal stability. These results indicated that Zn ions with relatively low reactivity surrounded the InAs surface and affected the

Fig. 3 Surface analyses of the InAs QDs synthesized with and without the zinc coordination complex. a Zn 2p, **b** In 3d, and **c** As 3d XPS spectra for both InAs and the InAs:Zn QDs.

growth rate of the InAs QDs, thereby narrowing the size distribution.

Based on the different size distribution seen without alloying, we can assume that the $ZnCl_2$-TOP precursor played a critical role in nucleation and growth of the InAs QDs. We measured the absorption spectra of aliquots extracted at different reaction temperatures during the syntheses of InAs (Fig. 2e) and InAs:Zn (Fig. 2f). In the case of InAs:Zn QDs, the nuclei began to form at 200 °C, whereas in the conventional synthesis of the InAs QDs, the absorption shoulder barely appeared at 220 °C. This meant that the $ZnCl_2$-TOP precursor readily reacted with the indium and arsenic precursors and simultaneously formed nuclei. After the nucleation process, InAs grew as the reaction temperature increased, but the absorption peak continued to shift and broaden, indicating that the size distribution of the InAs QDs was poor because the growth rates of most nuclei formed at the different temperatures were similar (Fig. 2e)[12,18]. However, with the InAs:Zn QDs, the excitonic peak moved toward a longer wavelength and was simultaneously narrowed and focused (Fig. 2f). This evolution of the absorption spectrum supported our hypothesis that the $ZnCl_2$-TOP precursor formed Zn-As intermediates and aided the InAs nucleation process as well as size focusing during the growth process.

We conducted additional control experiments using other reagents, including $ZnCl_2$-oleylamine, $ZnCl_2$-TOP and TOP alone (Fig. S5a). When the $ZnCl_2$-oleylamine was added, the absorption peak was broader than that of the conventional InAs QDs. We speculate that the $ZnCl_2$-oleylamine complex readily decomposed into Zn ions even at low temperatures, which had a radical effect on

InAs nucleation. On the other hand, similar absorption curves were obtained when only TOP was used without $ZnCl_2$, indicating that TOP itself did not play a significant role in the nucleation and growth of InAs. To compare the thermal stabilities of the molecules, we conducted thermogravimetric analyses of $ZnCl_2$-TOP and TOP (Fig. S5b). The $ZnCl_2$-TOP precursor was quite stable up to ~240 °C, while TOP began to decompose at ~200 °C. Based on these results, we hypothesize that the $ZnCl_2$-TOP precursor formed Zn-As intermediates that aided in the nucleation and size focusing processes occurring during particle growth. These findings suggested that the $ZnCl_2$-TOP precursor was required for the synthesis of uniform InAs QDs exhibiting a high PLQY.

We analyzed the chemical compositions of the InAs and InAs:Zn QDs using X-ray photoemission spectroscopy (XPS). First, a clear difference appeared in the Zn 2p peaks located at 1045 and 1021.9 eV, which were observed only for the InAs:Zn QD samples (Fig. 3a). This also revealed the presence of Zn on the surfaces of the InAs:Zn QDs. Because phosphorus from the TOP ligand, which was used to form the $ZnCl_2$-TOP complex, was not detected, it was confirmed that TOP acted as a weakly bound ligand or may have merely affected the reaction process[37] (Fig. S6). In the InAs QDs made with and without Zn precursors, the In $3d_{3/2}$ and $3d_{5/2}$ peaks were located at 451.9 and 444.3 eV, respectively. However, the full widths at half maximum (FWHM) of the In 3d bands for the InAs:Zn QDs were narrower than those of the bare InAs QDs, indicating the presence of In bonds other than the In-As bonds in the bare InAs QDs (Fig. 3b). The As 3d spectrum had peaks at 41.5 and 40.8 eV for the As $3d_{3/2}$ and $3d_{5/2}$ binding energies (Fig. 3c). However, we
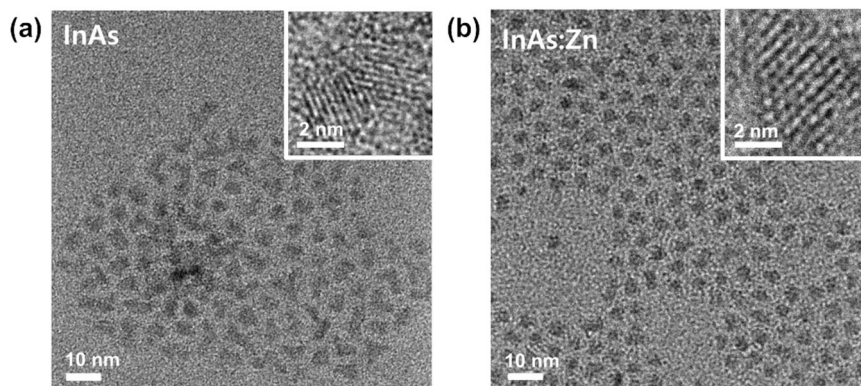
Fig. 4 Colloidal stability and size distribution of InAs and InAs:Zn QDs. TEM images of the InAs QDs made **a** without and **b** with the ZnCl$_2$-TOP complex.
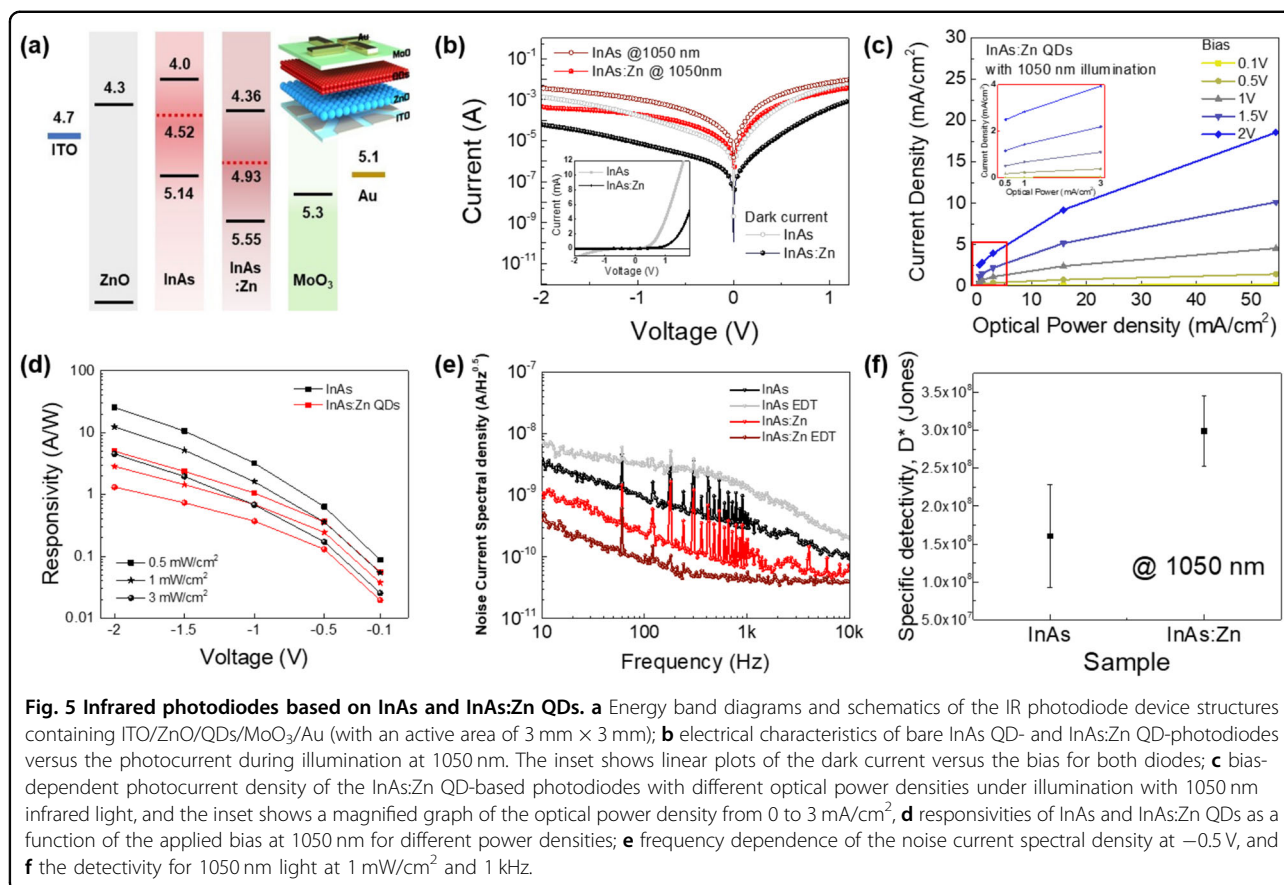
observed a shoulder peak near 43.8 eV for both the InAs and InAs:Zn samples, which presumably corresponded to unintentional surface oxidation of the As even though the synthesis was conducted under air-free conditions[16,24]. Notably, the area ratio of the As-O/As-In peaks decreased from 0.48 to 0.05 when using the Zn precursor. The reduced size of the As-O peak indicated that the added Zn precursor not only passivated the surfaces of InAs nuclei but also prevented surface oxidation, consistent with a previous report for InZnP[38]. If a large amount of Zn reacted with the In and As, there would have been a change in the binding energy of In or As; however, there was no peak shift for the InAs:Zn QDs. Only 2 at.% Zn was indicated by the ICP−OES analysis, and the unchanged XPS peaks also indicated that Zn was located at the surfaces of the InAs QDs. The addition of the ZnCl$_2$-TOP precursor, which increased the size uniformity and removed surface defects, consequently improved the optical properties of the InAs QDs, which was consistent with the narrow absorption and emission bands.

Additionally, removal of the surface oxidative species by the Zn precursors was found to improve the colloidal stability and dispersibility. In low- and high-resolution transmission electron microscopy (TEM) images, we observed differences in the sizes and shapes of the InAs QDs after the addition of the ZnCl$_2$-TOP precursor. The average diameter of InAs:Zn QDs was 4.35 ± 0.9 nm, slightly smaller than that of InAs QDs (4.7 ± 1.4 nm). As shown in Fig. 4a, the bare InAs QDs appeared to be unstable, poorly distributed, and agglomerated, resulting in irregular shapes. However, the narrow size distribution and stable dispersibility of the InAs:Zn QDs were attributed to the clean surfaces resulting from the Zn ions that acted as etchants for the surface oxide (Fig. 4b)[18]. As shown in Fig. S7, when approximately 100 particles were measured in each sample, the size distribution of the InAs:Zn QDs was narrower than that of the InAs QDs.

The photographs in Fig. S8 show InAs and InAs:Zn QD solutions two months after the syntheses. While the bare InAs QDs were aggregated to form gel-like states, the InAs QDs treated with the ZnCl$_2$-TOP precursor were well dispersed in colloidal form. In parallel with the XPS and ICP−OES results, it was noticed that the Zn precursors removed the surface oxides and prevented further oxide formation by surface passivation of the InAs QDs, providing a well-dispersed colloid. Based on previous research, the weakly bound oleylamine ligand was not sufficient to passivate the surfaces of III−V QDs; thus, Z-type ligands, such as oleic acid, may be needed[2,8,28]. The ZnCl$_2$-TOP complex and decomposed Zn ions may have acted as Z-type ligands because of their Lewis acidic nature. We believe that the ZnCl$_2$-TOP complex removed the surface oxidative species from the InAs QDs and enhanced the dispersibility and colloidal stability of the InAs QDs, enabling subsequent infrared device fabrication via a solution process.

Notably, the zinc precursors on the InAs surfaces tuned the electronic states of the InAs QDs. We confirmed the band energy levels of the InAs and InAs:Zn QD films with ultraviolet photoelectron spectroscopy (UPS) along with Tauc plots of the absorption spectra (Fig. S9). The InAs:Zn QD film exhibited a lower Fermi level (i.e., more likely intrinsic) at −4.93 eV with a conduction band minimum (CBM) at −4.36 eV and valence band maximum (VBM) at −5.55 eV, while the bare InAs QD film was more likely n-type with CBM, VBM, and work function levels at −4.0, −5.14, and −4.52 eV, respectively (Fig. 5a). The overall decreased energy levels of the InAs:Zn QDs indicated that the surface Zn ions acted as p-type dopants of InAs and electrically moved the Fermi level to a lower n-type energy level[38].

To confirm the improved optical properties and modified electronic structure of InAs:Zn QDs, we investigated the spectral responses of QD photodiodes with inverted

Fig. 5 Infrared photodiodes based on InAs and InAs:Zn QDs. a Energy band diagrams and schematics of the IR photodiode device structures containing ITO/ZnO/QDs/MoO$_3$/Au (with an active area of 3 mm × 3 mm); **b** electrical characteristics of bare InAs QD- and InAs:Zn QD-photodiodes versus the photocurrent during illumination at 1050 nm. The inset shows linear plots of the dark current versus the bias for both diodes; **c** bias-dependent photocurrent density of the InAs:Zn QD-based photodiodes with different optical power densities under illumination with 1050 nm infrared light, and the inset shows a magnified graph of the optical power density from 0 to 3 mA/cm^2, **d** responsivities of InAs and InAs:Zn QDs as a function of the applied bias at 1050 nm for different power densities; **e** frequency dependence of the noise current spectral density at −0.5 V, and **f** the detectivity for 1050 nm light at 1 mW/cm^2 and 1 kHz.

structures consisting of ITO/ZnO/QDs/MoO$_3$/Au (Fig. 5a). We observed the current density–voltage (J–V) characteristics of two photodiodes with 3 × 3 mm IR active areas containing bare InAs or InAs:Zn QDs under illumination with 1050 nm infrared light. Because the ligand exchange process may have altered the effects of the surface-attached Zn, relatively thin QD films were fabricated without a ligand exchange process for a proof-of-concept demonstration (Fig. 5b). In the diode based on the InAs:Zn QD film, the dark current was approximately 7 μA at −1 V, which was more than approximately two orders of magnitude lower than that of the photodiode based on the bare InAs QDs. The InAs:Zn QD diode demonstrated more ideal behavior and less ohmic/nonohmic leakage current than the InAs QD diode, which was attributed to the removed defect states and reduced recombination centers[3]. Given that Zn surface doping shifted the Fermi level of the InAs QDs close to the intrinsic level, the overall structure was close to a p-i-n structure with n-type ZnO and p-type MoOx layers. Figure S10 shows the overall I–V characteristics of the InAs QDs and InAs:Zn QDs with an applied bias from −2 to 2 V at different wavelengths and as a function of the optical power density for 1050 nm illumination. Distinctively, the InAs:Zn QDs exhibited a lower dark current with our device structure.

We also tested photodiodes with either InAs or InAs:Zn QD films after replacing the native oleylamine with ethanedithiol (EDT) (Fig. S11). EDT is a relatively short molecule with S atoms at each end, and these can act as donors to InAs. In the photocurrent plots, InAs QD photodiodes treated with EDT showed metallic characteristics, as the EDT led to degenerate n-type InAs (Fig. S11a). However, InAs:Zn QDs treated with EDT produced much lower dark currents and leakage currents in the photodiodes than the InAs QDs, possibly due to the Zn ions on the surfaces of the InAs QDs (Fig. S11b). The dark current for InAs:Zn with the EDT treatment was approximately an order of magnitude higher than that of the InAs:Zn photodiode without the EDT treatment, suggesting that improvement and optimization of the ligand exchange process is needed. However, we confirmed that the surface Zn ion acceptors affected the electronic states of the InAs QDs by adjusting the carrier concentration and Fermi levels and consequently blocking back injection of the carriers to the electrodes.

Based on the frequency responses of the photodiodes under the NIR laser diode (Fig. S12), the 3 dB cutoff frequency of the InAs:Zn QD photodiode exceeded 100 kHz, whereas that of the bare InAs QD photodiode was 69 kHz. The fast response was also attributed to elimination of the

surface oxidized defects by the Zn precursors. Figure 5c shows the bias-dependent photocurrent densities of the InAs:Zn QD photodiodes measured at 1050 nm with different optical power densities. As the bias was increased, the photocurrent increased linearly with the optical power density. Limited absorption by the thin QD layers caused a decrease in the photocurrent increase at high photon flux; further development and optimization of the device fabrication process is still needed. However, the InAs:Zn QDs effectively generated photocarriers by absorbing 1050 nm light and transferring them without severe recombination. Figure 5d–f depicts the responsivities (R), noise spectral densities (NSD), and specific detectivities (D^*) of the photodiodes containing InAs and the InAs:Zn QDs. The responsivity, R, was calculated with the equation $R = I_{ph}/P_0 = (I_{light} - I_{dark})/P_0$, where I_{ph} is the photocurrent, I_{light} is the current in the illuminated state, I_{dark} is the dark current, and P_0 is the optical power incident on the photodiode. D^* was calculated with the equation $D^* = \sqrt{AB}/\text{NEP}$, where A is the active device area, B is the electrical bandwidth, and NEP is the noise equivalent power. Figure 5d shows the responsivity as a function of applied bias at a wavelength of 1050 nm for different power densities. The InAs QD photodiode, which had a relatively high dark current value, showed a higher overall responsivity than the InAs:Zn QD photodiode. Figure 5e shows the noise characteristics of the InAs QD photodiodes with and without the Zn precursor. The NSD was associated with dark current and was affected by the surface traps[39,40]. The photodiodes containing InAs QDs had a high NSD value, especially for the InAs with the EDT treatment, due to their high darks current mentioned above. However, the NSD value of InAs:Zn QDs was approximately five times lower than that of the InAs QDs at 1 kHz since the Zn precursor removed the traps in the InAs QD surface. In Fig. 5f, the detectivity of the InAs QD-photodiode at a 1050 nm wavelength was 1 mW/cm^2 at 1 kHz. Despite the relatively low responsivity, the InAs:Zn QD photodiodes showed a higher D^* of $2.98 \pm 0.46 \times 10^8$ Jones, which was twice as high as that of the InAs QD-photodiode with a value of $1.60 \pm 0.68 \times 10^8$ Jones. Based on these results, the InAs:Zn QD film exhibited a low dark current as well as a sufficiently high performance compared to the bare InAs QD film, as removal of the surface defects inhibited trapping of the photogenerated carriers. Our synthetic strategy involving the ZnCl$_2$-TOP complex improved the quality of the colloidal InAs QDs and promises opportunities for using InAs QDs in fast and highly sensitive IR detectors.

Conclusion

We reported a novel strategy for synthesizing infrared-active InAs QDs by using a zinc-based coordination complex. The proposed ZnCl$_2$-TOP reaction additive imparted chemical and electrical effects on the InAs QDs.

The Zn precursors injected during the coreduction reaction improved the size homogeneity of the InAs QDs without an additional size-selection process, which was previously considered essential. Moreover, the addition of the Zn precursor reduced the extent of oxidation on the InAs QDs and improved their optical properties as well as their chemical/colloidal stabilities. The surface-attached Zn modulated the electrical properties and energy levels of the InAs QD films. We designed proof-of-concept QD photodiodes without ligand exchange processes to identify the electrical characteristics of the InAs:Zn QDs. We confirmed that Zn passivation negated the effects of the n-type InAs QDs, resulting in energy levels that were well matched with those of the n-type ZnO and p-type MoO$_3$ layers in an IR photodiode device and improved the electrical properties. The InAs:Zn QD photodiode exhibited a dark current that was two orders of magnitude lower and a faster response time than bare InAs QD-based photodiodes prepared without ligand exchange. We anticipate that our unique synthetic approach to InAs QDs with a chemically and electrically active Zn precursor will inspire new directions for III-V QD-based NIR and SWIR applications.

Author contributions
S.K., S.Y.: conceptualization, methodology, investigation, formal analysis, visualization, data curation, and writing—original draft. M.L., J.J., S.S., and N.G.: formal analysis and investigation. I.J. and H.J.: resource and visualization, G.W.H.: conceptualization and writing—review, N.O.: conceptualization, visualization, supervision, funding acquisition, project administration, and writing—review and editing.

Conflict of interest
The authors declare no competing interests.

References
1. Del Alamo, J. A. Nanometre-scale electronics with III-V compound semi-conductors. *Nature* **479**, 317–323 (2011).
2. De Mello Donega, C. et al. Luminescent colloidal InSb quantum dots from in situ generated single-source precursor. *ACS Nano* **14**, 13146–13160 (2020).
3. Kagan, C. R., Lifshitz, E., Sargent, E. H. & Talapin, D. V. Building devices from colloidal quantum dots. *Science* **353**, aac5523 (2016).
4. Dai, X. et al. Solution-processed, high-performance light-emitting diodes based on quantum dots. *Nature* **515**, 96–99 (2014).

5. Brown, P. R. et al. Energy level modification in lead sulfide quantum dot thin films through ligand exchange. *ACS Nano* **8**, 5863–5872 (2014).

6. Medintz, I. L., Uyeda, H. T., Goldman, E. R. & Mattoussi, H. Quantum dot bioconjugates for imaging, labelling and sensing. *Nat. Mater.* **4**, 435–446 (2005).

7. Voznyy, O. et al. Machine learning accelerates discovery of optimal colloidal quantum dot synthesis. *ACS Nano* **13**, 11122–11128 (2019).

8. Rogach, A. L., Eychmüller, A., Hickey, S. G. & Kershaw, S. V. Infrared-emitting colloidal nanocrystals: Synthesis, assembly, spectroscopy, and applications. *Small* **3**, 536–557 (2007).

9. Sun, B. et al. Fast near-infrared photodetection using III–V colloidal quantum dots. *Adv. Mater.* **34**, 1–9 (2022).

10. Lu, H., Carroll, G. M., Neale, N. R. & Beard, M. C. Infrared quantum dots: progress, challenges, and opportunities. *ACS Nano* **13**, 939–953 (2019).

11. Tamang, S., Lincheneau, C., Hermans, Y., Jeong, S. & Reiss, P. Chemistry of InP nanocrystal syntheses. *Chem. Mater.* **28**, 2491–2506 (2016).

12. Franke, D. et al. Continuous injection synthesis of indium arsenide quantum dots emissive in the short-wavelength infrared. *Nat. Commun.* **7**, 1–9 (2016).

13. TaMang, S., Lee, S., Choi, H. & Jeong, S. Tuning size and size distribution of colloidal InAs nanocrystals via continuous supply of prenucleation clusters on nanocrystal seeds. *Chem. Mater.* **28**, 8119–8122 (2016).

14. Srivastava, V., Janke, E. M., Diroll, B. T., Schaller, R. D. & Talapin, D. V. Facile, economic and size-tunable synthesis of metal arsenide nanocrystals. *Chem. Mater.* **28**, 6797–6802 (2016).

15. Srivastava, V., Dunietz, E., Kamysbayev, V., Anderson, J. S. & Talapin, D. V. Monodisperse InAs quantum dots from aminoarsine precursors: understanding the role of reducing agent. *Chem. Mater.* **30**, 3623–3627 (2018).

16. Song, J. H., Choi, H., Pham, H. T. & Jeong, S. Energy level tuned indium arsenide colloidal quantum dot films for efficient photovoltaics. *Nat. Commun.* **9**, 1–9 (2018).

17. Kim, Y. et al. III–V colloidal nanocrystals: control of covalent surfaces. *Chem. Sci.* **11**, 913–922 (2020).

18. Koh, S. et al. Zinc-phosphorus complex working as an atomic valve for colloidal growth of monodisperse indium phosphide quantum dots. *Chem. Mater.* **29**, 6346–6355 (2017).

19. Kirkwood, N. et al. Locating and controlling the Zn content in In(Zn)P quantum dots. *Chem. Mater.* **32**, 557–565 (2020).

20. Pietra, F. et al. Tuning the lattice parameter of InxZnyP for highly luminescent lattice-matched core/shell quantum dots. *ACS Nano* **10**, 4754–4762 (2016).

21. Thuy, U. T. D., Reiss, P. & Liem, N. Q. Luminescence properties of In(Zn)P alloy core/ZnS shell quantum dots. *Appl. Phys. Lett.* **97**, 1–4 (2010).

22. Song, W. S. et al. Amine-derived synthetic approach to color-tunable InP/ZnS quantum dots with high fluorescent qualities. *J. Nanopart. Res.* **15**, 1750 (2013).

23. Norris, D. J., Efros, A. L. & Erwin, S. C. Doped nanocrystals. *Sci* **319**, 1776–1779 (2008).

24. Asor, L. et al. InAs nanocrystals with robust p-type doping. *Adv. Funct. Mater.* **2007456**, 2007456 (2020).

25. Koh, W. et al. Energetic sulfide vapor-processed colloidal InAs quantum dot solids for efficient charge transport and photoconduction. *Adv. Photonics Res.* **2100243**, 2100243 (2021).

26. Wijaya, H. et al. Efficient near-infrared light-emitting diodes based on In(Zn)As–In(Zn)P–GaP–ZnS quantum dots. *Adv. Funct. Mater.* **30**, 1–7 (2020).

27. Zhu, D. et al. ZnCl$_2$-mediated synthesis of InAs nanocrystals with aminoarsine. *J. Am. Chem. Soc.* **144**, 10515–10523 (2022).

28. Zhao, T. et al. General synthetic route to high-quality colloidal III-V semiconductor quantum dots based on pnictogen chlorides. *J. Am. Chem. Soc.* **141**, 15145–15152 (2019).

29. Gilroy, K. D., Ruditskiy, A., Peng, H. C., Qin, D. & Xia, Y. Bimetallic nanocrystals: syntheses, properties, and applications. *Chem. Rev.* **116**, 10414–10472 (2016).

30. Jang, E., Kim, Y., Won, Y. H., Jang, H. & Choi, S. M. Environmentally friendly InP-based quantum dots for efficient wide color gamut displays. *ACS Energy Lett.* **5**, 1316–1327 (2020).

31. Heath, J. R. & Shiang, J. J. Covalency in semiconductor quantum dots. *Chem. Soc. Rev.* **27**, 65–71 (1998).

32. Calvin, J. J. et al. Thermodynamic investigation of increased luminescence in indium phosphide quantum dots by treatment with metal halide salts. *J. Am. Chem. Soc.* **142**, 18897–18906 (2020).

33. Hogg, J. M. et al. Liquid coordination complexes of Lewis acidic metal chlorides: Lewis acidity and insights into speciation. *Dalton Trans.* **46**, 11561–11574 (2017).

34. Ovchinnikov, A., Smetana, V. & Mudring, A. V. Metallic alloys at the edge of complexity: structural aspects, chemical bonding and physical properties. *J. Phys. Condens. Matter* **32**, 243002 (2020).

35. Turbervill, R. S. P. & Goicoechea, J. M. From clusters to unorthodox pnictogen sources: solution-phase reactivity of [E7]3-(E = P-Sb) anions. *Chem. Rev.* **114**, 10807–10828 (2014).

36. Dalpian, G. M. & Chelikowsky, J. R. Self-purification in semiconductor nanocrystals. *Phys. Rev. Lett.* **96**, 1–4 (2006).

37. Fisher, A. A. E., Osborne, M. A., Day, I. J. & Lucena Alcalde, G. Measurement of ligand coverage on cadmium selenide nanocrystals and its influence on dielectric dependent photoluminescence intermittency. *Commun. Chem.* **2**, 1–9 (2019).

38. Mordvinova, N. E., Vinokurov, A. A., Lebedev, O. I., Kuznetsova, T. A. & Dorofeev, S. G. Addition of Zn during the phosphine-based synthesis of indium phosphide quantum dots: doping and surface passivation. *Beilstein J. Nanotechnol.* **6**, 1237–1246 (2015).

39. Hooge, F. N. 1/f Noise Ssources. *IEEE Trans. Electron. Devices* **41**, 1926–1935 (1994).

40. Manders, J. R. et al. Low-noise multispectral photodetectors made from all solution-processed inorganic semiconductors. *Adv. Funct. Mater.* **24**, 7205–7210 (2014).